JOURNAL OF SOLID STATE CHEMISTRY 84, 386–400 (1990)

Crystal Structure of the Ordered $Nb_{10}Ge_7$ Phase

M. ARITA* AND H.-U. NISSEN

Laboratorium für Festkörperphysik, ETH Zürich, CH-8093 Zürich, Switzerland

AND W. SCHAUER

Kernforschungszentrum Karlsruhe, Institut für Technische Physik, D-7500 Karlsruhe, Federal Republic of Germany

Received August 15, 1989; in revised form October 16, 1989

The structure of a new ordered phase, $Nb_{10}Ge_7$ (or $Nb_5Ge_3Ge_{0.5}$; trigonal), is described on the basis of electron microscopic and electron diffraction data. The new phase was found in a Nb–Ge tape prepared by the coevaporation technique. The new structure can be derived from the hexagonal $D8_8$-structure of Nb_5Ge_3 by periodically inserting Ge-atoms at octahedral sites. The lattice parameters of this structure can be described as follows, using the lattice parameters of the $D8_8$-structure

$$a = \sqrt{3} \cdot a_{Nb_5Ge_3(D8_8)} \quad \text{and} \quad c = c_{Nb_5Ge_3(D8_8)}$$

in hexagonal description. The grains of this phase are usually elongated along the c-direction. Structural data of the new phase:

$Nb_{10}Ge_7$, trigonal, $hP51$, $P\bar{3}2/m1$, $a = 1.337$ nm, $c = 0.537$ nm, $Z = 3$, $V_{Nb_{10}Ge_7} \approx 3V_{Nb_5Ge_3(D8_8)}$.

The structure represents a new structure type with an ordered atom arrangement, intermediate between the Mn_5Si_3 type and the Ti_5Ga_4 type, in which the octahedral sites are only partly occupied.

1. Introduction

Besides the X-ray diffraction techniques, transmission electron microscopy (TEM) has contributed to the determination of crystal structures. The latter method is very efficient especially for small crystals, typically less than 1 μm in diameter. In this work, electron microscopic imaging and diffraction techniques are applied to a new ordered phase, $Nb_5Ge_3Ge_{0.5}$, which is frequently observed in Nb–Ge evaporated material with 40.1 at.% Ge.

In the Nb–Ge compound system, the hexagonal $D8_8$-phase (space group $P6_3/mcm$; (*1, 2*)) has been reported to appear for germanium concentrations ranging between 38 and 44 at.%. Therefore the chemical formula of this phase can be expressed as Nb_5Ge_3 (37.5 at.% Ge), Nb_3Ge_2 (40.0 at.% Ge), or $Nb_{10}Ge_7$ (41.2 at.% Ge) (e.g., (*3*)). The crystal structure of Nb_5Ge_3 having the $D8_8$-structure is shown in Fig. 1. For Nb_3Ge_2 and $Nb_{10}Ge_7$ materials, the excess Ge atoms are randomly distributed at octa-

* Present address: International Research Laboratories, Ciba-Geigy Japan, Takarazuka, Hyogo, 665 Japan.

0022-4596/90 $3.00

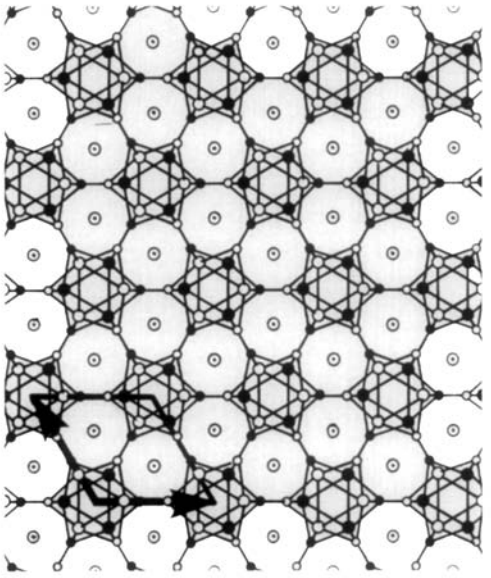

Fig. 1. Structure model of Nb_5Ge_3 with the $D8_8$-structure, projected onto the (00·1)-plane. The small and large circles denote Ge- and Nb-atoms, respectively. Black and white circles indicate atoms at $z = 0$ and $\frac{1}{2}$, respectively. Circles with dots are Nb-atoms at $z = \pm\frac{1}{4}$ forming the Nb-chains along the [00·1]-direction. The parallelogram indicates the unit cell. The octahedral sites are at the corners of the parallelogram.

hedral sites (2*d*-sites) of Nb_5Ge_3 with the $D8_8$-structure (*4–6*). This site is surrounded by six Nb atoms. When the germanium occupancies at all octahedral sites are equal to one, the structure corresponds to the Ti_5Ga_4 type (*7*).

The $D8_8$-phase has been reported to be stabilized by metalloid atoms such as C, B, N, and O (*1, 2, 8*) and the resulting structures are referred to as Nowotny phases (*9–11*). Similar phenomena have been observed also in the Nb–Ga and V–Ga compound systems (*12–14*). On the other hand, it has been reported that the $D8_8$-phase can be synthesized under clean conditions (*4, 15–18*). Kloska and Haase, on the basis of their carbon implantation experiments (*3*), concluded that the $D8_8$-phase of Nb–Ge is either stabilized by light elements or metastable.

2. Experimental Procedure

The Nb–Ge specimens used in this work were prepared as tapes by the coevaporation method using pure Nb (MARZ grade, Material Research Corporation) and pure Ge (99.999%, semiconductor purity). Vapors of these elements were deposited onto a polycrystalline molybdenum substrate kept at about 1.10×10^3 K (~850°C). The vacuum during the evaporation was of the order of 10^{-6} Pa ($\sim 10^{-8}$ Torr). The germanium concentration of the tape was 40.1 at.%.

For electron microscopic observations, the Nb–Ge tape was chemically etched using a $FeCl_3$ and HF hydrous solutions (*19–20*). The etched specimens were observed using a JEOL JEM 200 CX electron microscope equipped with a top-entry tilting goniometer (±10°, $C_S = 1.2$ mm) as well as by a JEOL JEM 100 C instrument with a side entry goniometer (±60°). In order to take high resolution electron microscopic (HREM) images, only the diffraction spots with space frequencies smaller than 4.3 nm^{-1} were used.

3. General Remarks

In the specimen used in this work (40.1 at.% Ge), grains with a rectangle diffraction pattern (Fig. 2a) were commonly observed. The *d*-value of the spots A and B in this figure are 0.389 and 0.267 nm, respectively. These values correspond well to those of $(11{\cdot}0)_{D8_8}$ (0.386 nm) and $(00{\cdot}2)_{D8_8}$ (0.269 nm), respectively (*2*). The subscripts mean that these indices are those of the $D8_8$-structure. The diffraction spots indicated by arrows correspond to reciprocal lattice points of the $D8_8$-structure. In addition a set of spots occur along the $(11{\cdot}0)_{D8_8}$-direction. The spots nearest to the center correspond to $\pm\frac{1}{3} \cdot (11{\cdot}0)_{D8_8}$ whose *d*-value is 1.16 nm. This diffraction pattern cannot be explained by a superposition and multiple scattering of Nb_5Ge_3 with the tetragonal $D8_m$ (W_5Si_3

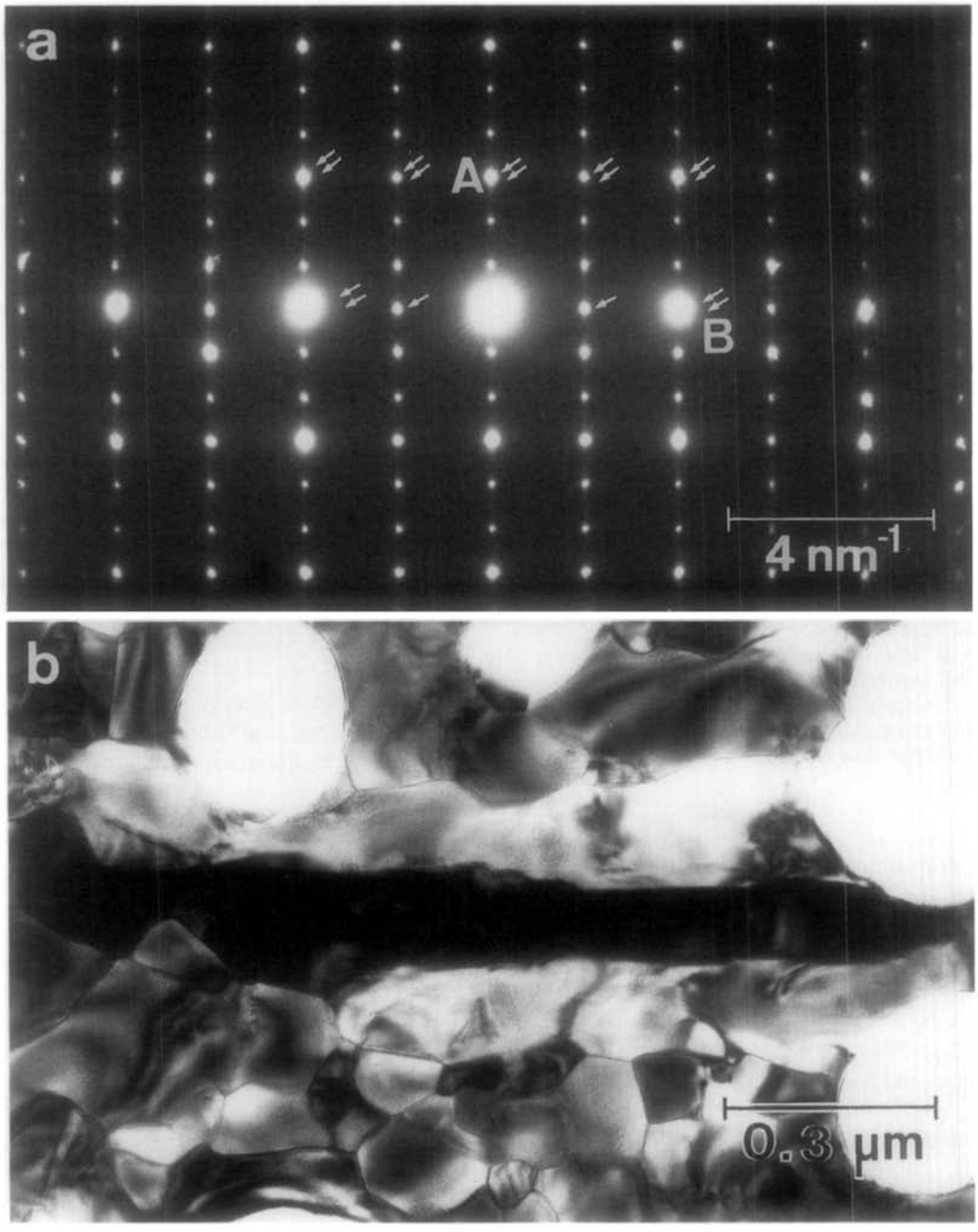

FIG. 2. (a) A typical electron diffractogram of the new phase. The arrowed spots correspond to the reciprocal lattice points of the $D8_8$-structure. Positions with single arrows have no intensities by kinematical diffraction from the $D8_8$ structure. (b) Bright field image corresponding to (a). The elongated dark region is the grain giving the diffraction pattern shown in (a).

type), the hexagonal $D8_8$ structures, and/or Nb_3Ge. The additional spots are marked as "extra spots" in this work. Weak streaks observed along the vertical direction indicate the existence of planar defects.

Figure 2b shows a bright field image of this material. The dark area is the grain showing the diffraction pattern of Fig. 2a. The grain is elongated along the direction of the B-reflection ($[00\cdot1]_{D8_8}$). The elongation is commonly recognized for grains showing the same diffraction patterns. This type of microstructure has also been observed in small particles of $V_5Si_3(D8_8)$ (*21*).

4. Electron Diffraction

In order to investigate the reciprocal lattice, diffraction patterns were taken after rotating the crystals (Figs. 3 and 4: some of the diffractograms contain reflections due to superposed adjacent grains). In Fig. 3, fourteen diffraction patterns with different orientations, (a) to (h), are shown. Some of these deviate from the axial orientation conditions because of the rotation limit of the instrument. The relatively strong diffraction spots in Fig. 3 correspond to those of the $D8_8$-phase. Because of the similarity in the diffraction pattern and in the microstructure reported above, the grain observed in Fig. 2 and the $D8_8$-phase must be related to each other. Assuming that the crystal structure studied here has a superlattice of the $D8_8$-phase, the lattice parameters of the $D8_8$-sublattice are obtained as $a = 0.775 \pm 0.005$ nm and $c = 0.540 \pm 0.020$ nm. The values reported earlier for the $D8_8$-phase are $a = 0.7718$ nm and $c = 0.5370$ nm (*2*). The "extra spots" mentioned above are observed at positions which have distances from the $D8_8$-spots of $\pm\frac{1}{3} \cdot (11\cdot0)_{D8_8}$. In Figs. 3A-b and 3B-d, the diffraction spots indicated by arrows cannot be explained by reciprocal lattice points on the 0th order Laue zone. These spots are contributions from the 1st order Laue zone, as described later.

In Fig. 4, the crystal is rotated up to 71° around $[00\cdot1]_{D8_8}$. The direction of observation for Fig. 4a is the same as that of Fig. 3a. After a 60° rotation, the same pattern was observed (Fig. 4e); this means that the "extra spots" could equally be observed from another $\langle11\cdot0\rangle_{D8_8}$-direction.

From these two experiments, it is concluded that the reciprocal space of this material has spots of the $D8_8$-phase and the "extra spots" located at the mass centers of the triangles formed by $D8_8$-spots. Therefore, the unit reciprocal vectors of this material are taken as $a^* = \frac{1}{3} \cdot (21\cdot0)_{D8_8}$, $b^* = \frac{1}{3} \cdot (11\cdot0)_{D8_8}$, and $c^* = (00\cdot1)_{D8_8}$. This selection of reciprocal axes corresponds to the following relation in real space:

$$a = a_{D8_8} - b_{D8_8}, \quad b = a_{D8_8} + 2b_{D8_8}, \quad c = c_{D8_8}. \quad (1)$$

The structure is thus hexagonal or trigonal. In the continuation of this paper all indices will be described using these lattice vectors.

Using this unit cell, the l-parameters of the reflections in Fig. 3 are 0 for the spots on the rotation axis, 1 for the spots on the first row from the rotation axis, 2 for the second row of spots from the rotation axis, etc.; an exception is Fig. 3F-n where the l-parameter of all reflections is 0.

Information about the structure is obtained from Fig. 3F. While Fig. 3F-k shows "extra spots" on the rotation axis ($l = 0$) and on the next rows of diffraction spots from the rotation axis ($l = 1$), Fig. 3F-n has no extra spots at the mass centers of the triangles. [A diffraction pattern with "extra spots" was also observed under this condition. Its occurrence may depend on the degree of order and/or difference in the structure. In this work, only the case with no "extra spots" at $l = 0$ is treated.] Since all of the reflections in Fig. 3F-n have $l = 0$, it

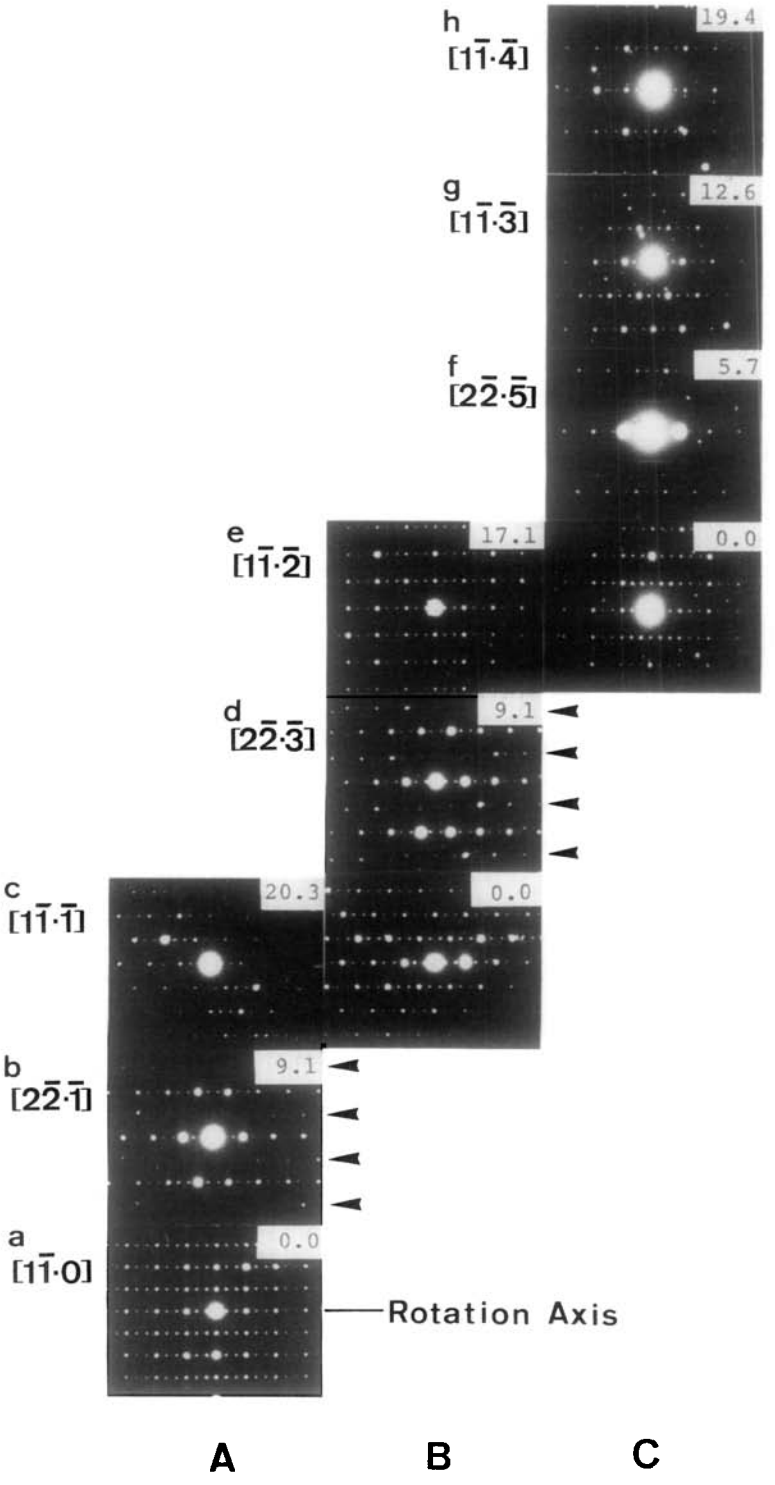

FIG. 3. Selected area electron diffractograms of six grains, (A) to (F), made after rotation. The rotation axis is the A-direction of Fig. 2a. The number in each figure is the rotation angle from the lowest pattern in each column. Incident beam directions are described by using the $D8_8$-indices. Arrowed spots are from the first Laue zone.

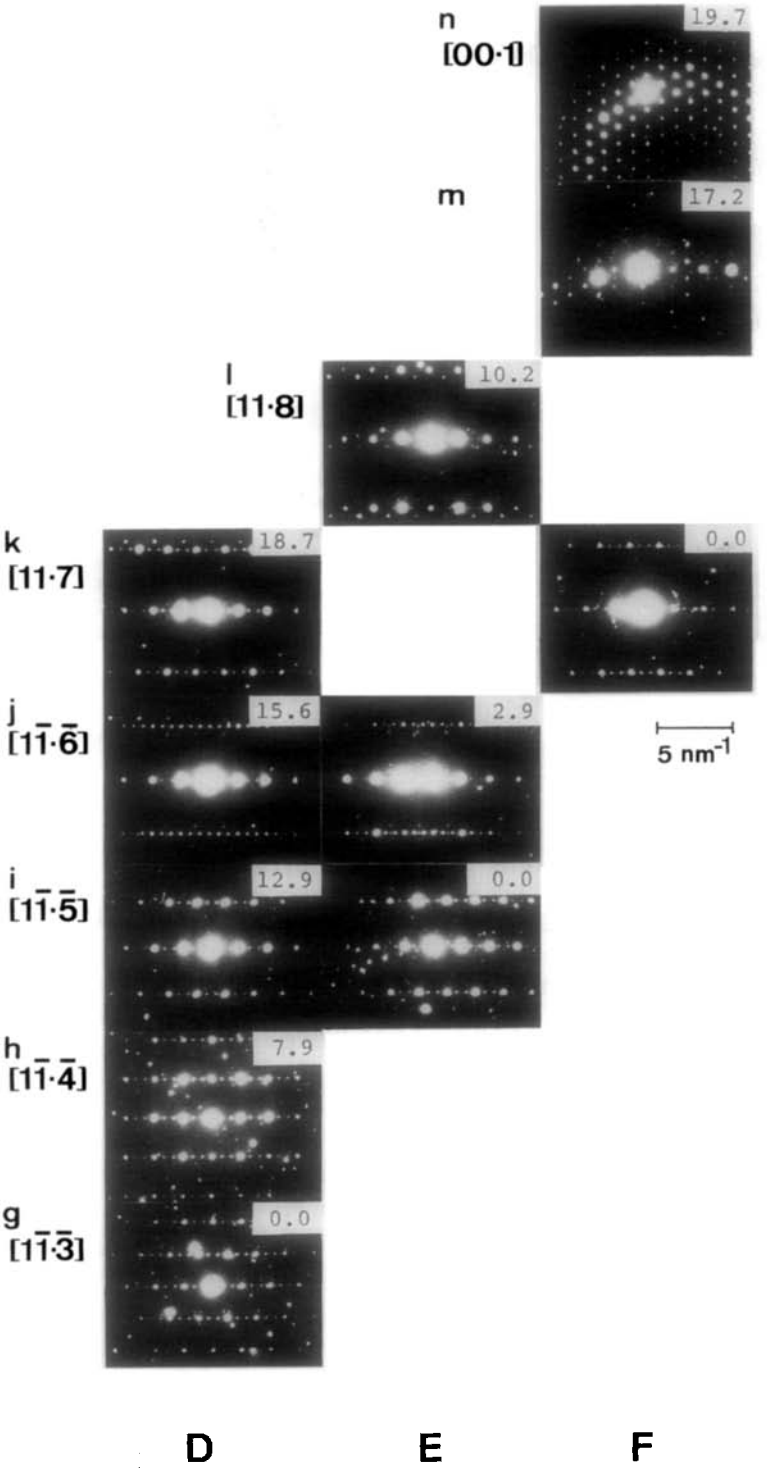

FIG. 3—*Continued*

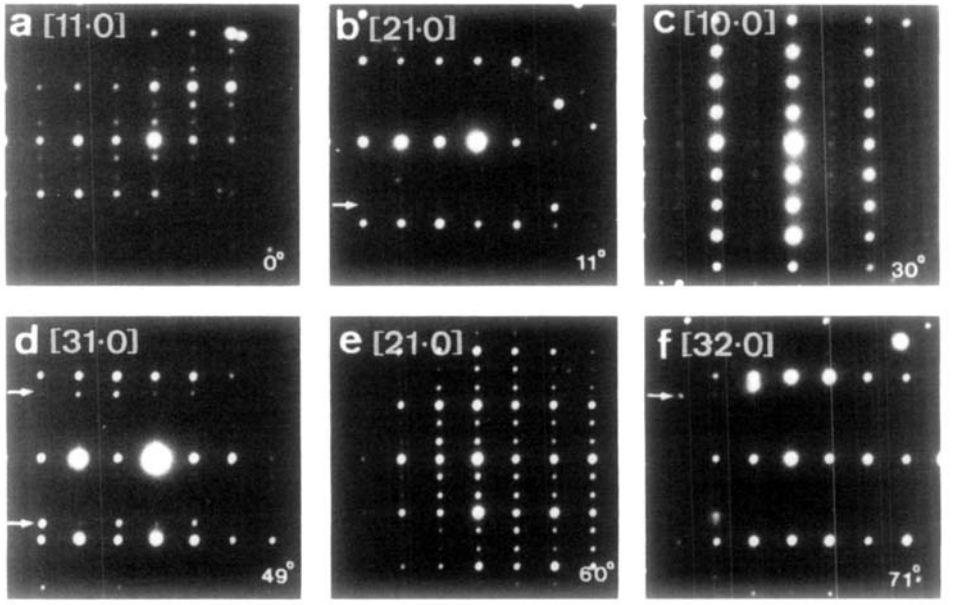

FIG. 4. Electron diffractograms rotated around the B-direction of Fig. 2a. The angles of rotation are shown against (a) 0°, (b) 11°, (c) 30°, (d) 49°, (e) 60°, and (f) 71°. The indices are those of the incident beam directions referred to the $D8_8$-structure. Spots indicated by arrows are contributions from the first order Laue zone.

can be concluded that the reciprocal plane with $l = 1$ has "extra spots" but not the one with $l = 0$. Thus the "extra spots" with $l = 0$ observed in the diffractograms were caused by the multiple scattering.

5. Crystal Structure Model

The following assumptions are used for the construction of a structure model:

(a) The new phase contains only Nb- and Ge-atoms, since the specimen was made under clean conditions.

(b) The germanium concentration is close to that of the specimen tape (40.1 at.% Ge).

(c) The structure has a superlattice of the $Nb_5Ge_3(D8_8)$ structure. It is hexagonal or trigonal, and its unit cell is, for example, described by Eq. (1). Using the data of the $D8_8$-structure (*2*), the lattice parameters in hexagonal description are $a = 1.337$ and $c = 0.537$ nm.

(d) In order to cause the "extra spots" to occur, germanium atoms are regularly added at the octahedral sites of the Nb_5Ge_3 ($D8_8$) structure. In this work, the added Ge-atoms will be called Ge^{II} in order to distinguish them from the Ge-atoms belonging to the Nb_5Ge_3-phase with the $D8_8$-structure (Ge^{I}).

The unit cell of this material is shown as a large parallelogram in Fig. 5a and is compared to that of the $D8_8$-structure (small parallelogram. Ge^{II}-atoms can occupy the octahedral sites indicated by letters 1 to 6:

$$1: (0\ 0\ 0) \quad 2: (0\ 0\ \tfrac{1}{2}) \quad 3: (\tfrac{1}{3}\ \tfrac{2}{3}\ 0)$$

$$4: (\tfrac{1}{3}\ \tfrac{2}{3}\ \tfrac{1}{2}) \quad 5: (\tfrac{2}{3}\ \tfrac{1}{3}\ 0) \quad 6: (\tfrac{2}{3}\ \tfrac{1}{3}\ \tfrac{1}{2}).$$

The crystal structure factor (F) is

$$F(hk \cdot l) = F_{D8_8}(hk \cdot l) + F_{Ge}(hk \cdot l), \quad (2)$$

where the first term comes from the Nb_5Ge_3 ($D8_8$) sublattice and the second term from

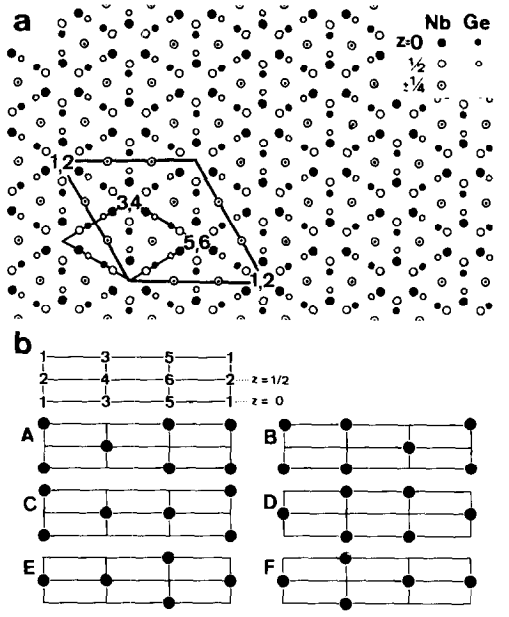

FIG. 5. (a) The unit cell of the new phase and the $D8_8$-phase (larger and smaller parallelograms, respectively) drawn onto the structure model of Nb_5Ge_3 ($D8_8$), projected onto (00.1)$D8_8$. Octahedral sites are marked by numbers 1 to 6 (1, 3, and 4: at $z = 0$, 2, 4, and 6: at $z = \frac{1}{2}$). (b) Possible configurations of Ge^{II}-atoms on (11·0) of the new unit cell. Corners of small rectangles are the octahedral sites.

the added Ge^{II} atoms. The parameters h, k, and l are based on the new unit cell

$$F_{Ge}(hk \cdot l) = \sum_{j=1}^{6} g_j f_{Ge} \exp\{2\pi i(hx_j + ky_j + lz_j)\}, \quad (3)$$

where f_{Ge} is the atomic scattering factor of Ge-atoms. Parameters g_j and $(x_j y_j z_j)$ are the occupancy of Ge^{II} and the positions of the jth octahedral site, respectively. The "extra spots" are at the reciprocal lattice points with $h - k = 3n \pm 1$ (n: integer). For these reflections, F_{D8_8} is zero. When l is zero, the "extra spots" have no intensities. Therefore,

$$\begin{aligned} F(h\ h - 3n \pm 1 \cdot 0) &= F_{Ge}(h\ h - 3n \pm 1 \cdot 0) \\ &= f_{Ge} \sum_{j=1}^{6} g_j \exp[2\pi i\{hx_j + (h - 3n \pm 1)y_j\}] \\ &= f_{Ge} \cdot [(g_1 + g_2) \\ &\quad + (g_3 + g_4) \exp\{2\pi i(h - 2n \pm \tfrac{2}{3})\} \\ &\quad + (g_5 + g_6) \exp\{2\pi i(h - n \pm \tfrac{1}{3})\}] \\ &= f_{Ge} \cdot \{(g_1 + g_2) + (g_3 + g_4) \exp\{\pm\tfrac{4}{3}\pi i) \\ &\quad + (g_5 + g_6) \exp(\pm\tfrac{2}{3}\pi i)\} \\ &= 0. \end{aligned} \quad (4)$$

Since this complex expression is zero, the real and the imaginary parts are zero, therefore

$$2(g_1 + g_2) = g_3 + g_4 + g_5 + g_6 \quad \text{[real part]} \quad (5)$$

and

$$g_3 + g_4 = g_5 + g_6 \quad \text{[imaginary part]}. \quad (6)$$

From Eqs. (5) and (6),

$$g_1 + g_2 = g_3 + g_4 = g_5 + g_6. \quad (7)$$

When l is one, the "extra spots" have intensities

$$\begin{aligned} F(h\ h - 3n \pm 1 \cdot 1) &= F_{Ge}(h\ h - 3n \pm 1 \cdot 1) \\ &= f_{Ge} \sum_{j=1}^{6} g_j \exp[2\pi i\{hx_j \\ &\quad + (h - 3n \pm 1)y_j + z_j\}] \\ &= f_{Ge} \cdot [(g_1 - g_2) \\ &\quad + g_3 \exp(\pm\tfrac{4}{3}\pi i) + g_4 \exp\{(\pm\tfrac{4}{3} + 1)\pi i\} \\ &\quad + (g_5 \exp\{\pm\tfrac{2}{3}\pi i) + g_6 \exp\{(\pm\tfrac{2}{3} + 1)\pi i\}] \\ &= f_{Ge} \cdot \{(g_1 - g_2) + (g_3 - g_4) \exp(\pm\tfrac{4}{3}\pi i) \\ &\quad + (g_5 - g_6) \exp(\pm\tfrac{2}{3}\pi i)\} \\ &\neq 0. \end{aligned} \quad (8)$$

Therefore, the real and/or the imaginary parts are not zero

$$2g_1 + g_4 + g_6 \neq 2g_2 + g_3 + g_5 \quad \text{[real part]} \quad (9)$$

and/or

$$g_3 + g_6 \neq g_4 + g_5 \quad \text{[imaginary part]}. \quad (10)$$

The structure model should satisfy Eq. (7) and Eqs. (9) and/or (10). When g_j (j = 1 to 6) is 0 or 1, six cases are possible. (In principle, structures with fractional g_j are also possible. In this case, the degree of order is low):

(A) $g_1 = g_4 = g_5 = 1$ and $g_2 = g_3 = g_6 = 0$

(B) $g_1 = g_3 = g_6 = 1$ and $g_2 = g_4 = g_5 = 0$

(C) $g_1 = g_4 = g_6 = 1$ and $g_2 = g_3 = g_5 = 0$

(D) $g_2 = g_3 = g_5 = 1$ and $g_1 = g_4 = g_6 = 0$

(E) $g_2 = g_4 = g_5 = 1$ and $g_1 = g_3 = g_6 = 0$

and

(F) $g_2 = g_3 = g_6 = 1$ and $g_1 = g_4 = g_5 = 0$.

In Fig. 5b, Ge^{II} positions on a (11·0)-plane are given. It is recognized that the structures (A) to (F) are identical; i.e., only one structure is possible when g_j is 0 or 1 (j = 1 to 6). The chemical formula is $Nb_{10}Ge_7$ (or $Nb_5Ge_3^{I}Ge_{0.5}^{II}$), with 41.16 at.% Ge. In the structure model, Ge^{II}-atoms form a triangle net with the edge of 1.337 nm at $z = 0$. At $z = \frac{1}{2}$, they form a honeycomb net with edge length 0.7718 nm. The crystal data are summarized in Table I. The Ge^{II}-atoms are at 2*d*- and 1*a*-sites.

In Fig. 6, electron diffraction patterns of Nb_5Ge_3($D8_8$) and the $Nb_{10}Ge_7$ ordered phase are kinematically calculated for comparison with Fig. 3. Only the spots on the 0th order Laue zone are shown. The model of the $Nb_{10}Ge_7$ ordered phase has "extra spots" only when l is odd. The "extra spots" with even l parameters which are recognized in Fig. 3 can be explained by the dynamical scattering effect; exceptions are Figs. 6b, 6d, and 6f.

TABLE I

CRYSTAL STRUCTURE DATA FOR ORDERED TRIGONAL $Nb_{10}Ge_7$

	x	y	z
Nb(1) in 6*i*	0.9167	0.0833	0.25
Nb(2) in 6*i*	0.5833	0.4167	0.25
Nb(3) in 6*i*	0.5	0.5	0.25
Nb(4) in 6*h*	0.3333	0	$\frac{1}{2}$
Nb(5) in 6*g*	0.3333	0	0
Ge(1) in 6*i*	0.7950	0.2050	0.25
Ge(2) in 6*i*	0.4167	0.5833	0.25
Ge(3) in 6*i*	0.1283	0.8717	0.25
Ge(4) in 2*d*	$\frac{1}{3}$	$\frac{2}{3}$	0.25
Ge(5) in 1*a*	0	0	0

Note. Space group $P\bar{3}m1$ (No. 164), a = 1.337 nm, and c = 0.537 nm.

Since Figs. 6b, 6d, and 6f contain reciprocal lattice points with even l-parameters only, the existence of the "extra spots" in the observations (Figs. 4b, 4d, and 4f) cannot be explained by multiple scattering among these reflections. In order to explain this contradiction, two examples containing reflections with larger d^*-values are shown in Fig. 7. The diffraction spots indicated by arrows cannot be recognized in the calculations. They are reflections with odd l-values from the first Laue zone: numbers in the figures indicate the l-parameters. The extra spots with even l-parameters can be produced by multiple scattering with the contribution from the spots on the first order Laue zone.

6. High Resolution Electron Microscopy

Figure 8a shows a structure image projected along [10·0] (= $[11\cdot0]_{D8_8}$), which was observed at the second bright thickness fringe. A laser optical diffractogram of the

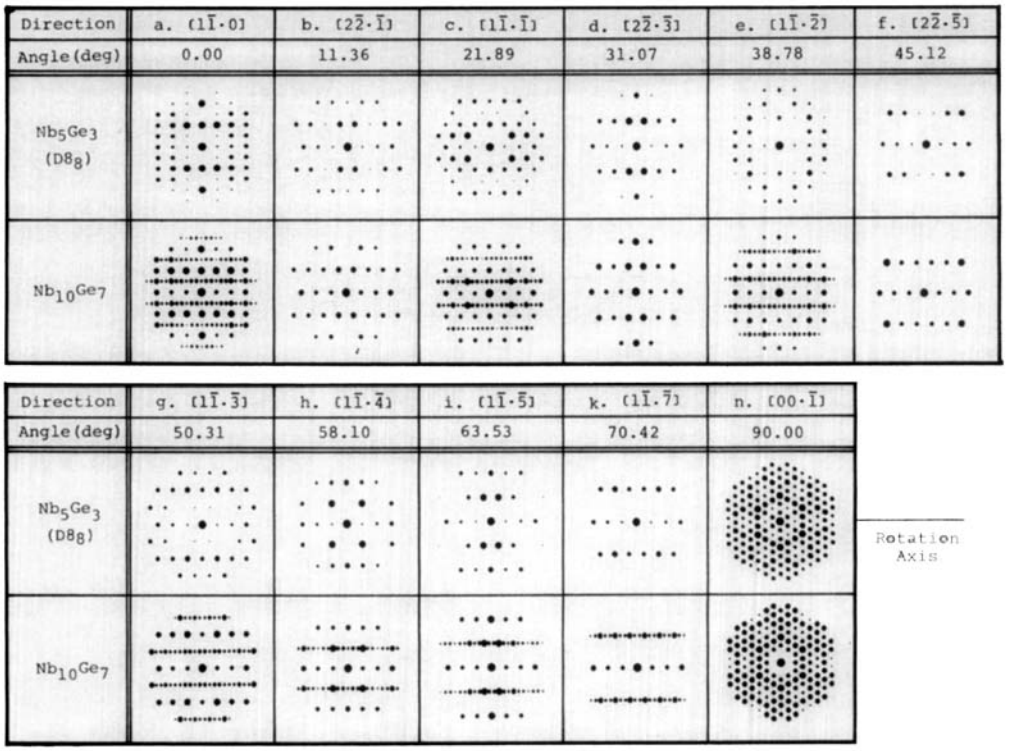

FIG. 6. Kinematical calculations of electron diffractograms corresponding to those in Fig. 3. The first and the second lines are for the incident beam directions using the indices and the rotation angles, respectively, of the $D8_8$ structure. For the ordered $Nb_{10}Ge_7$ phase, "extra spots" with odd l-parameters are seen.

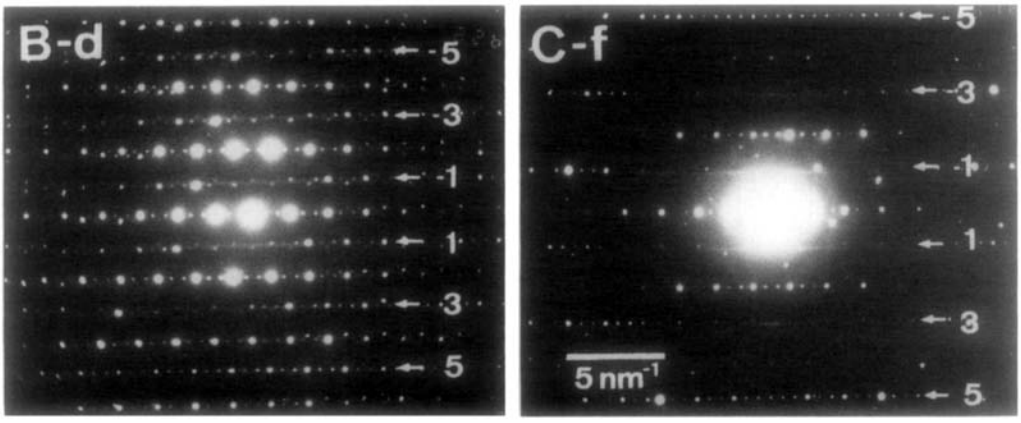

FIG. 7. Electron diffractograms of Figs. 3B-d and 3C-f. The arrowed reflection spots are from the first order Laue zone. The numbers are the l-parameters.

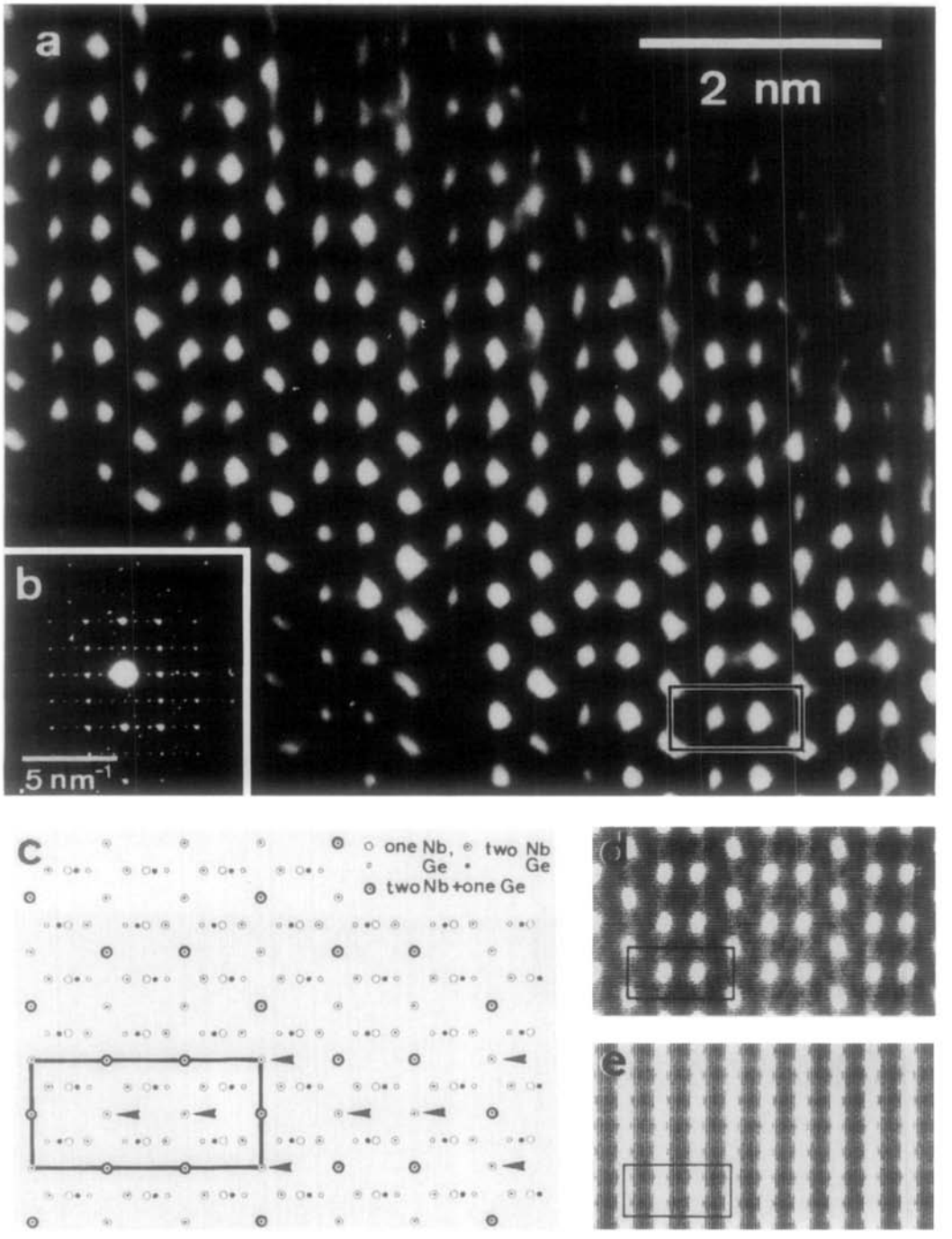

FIG. 8. (a) HREM image of the $Nb_{10}Ge_7$ ordered phase observed along [10·0]. (b) Corresponding electron diffractogram. (c) Structure model projected along [10·0]. (d) and (e) Calculated images for $Nb_{10}Ge_7$ ordered phase and $Nb_5Ge_3(D8_8)$, respectively, assuming an underfocus of 70 nm and a thickness of 18.72 nm. Rectangles in figures correspond to each other. Bright spots in (a) and (d) correspond to arrowed positions in (c).

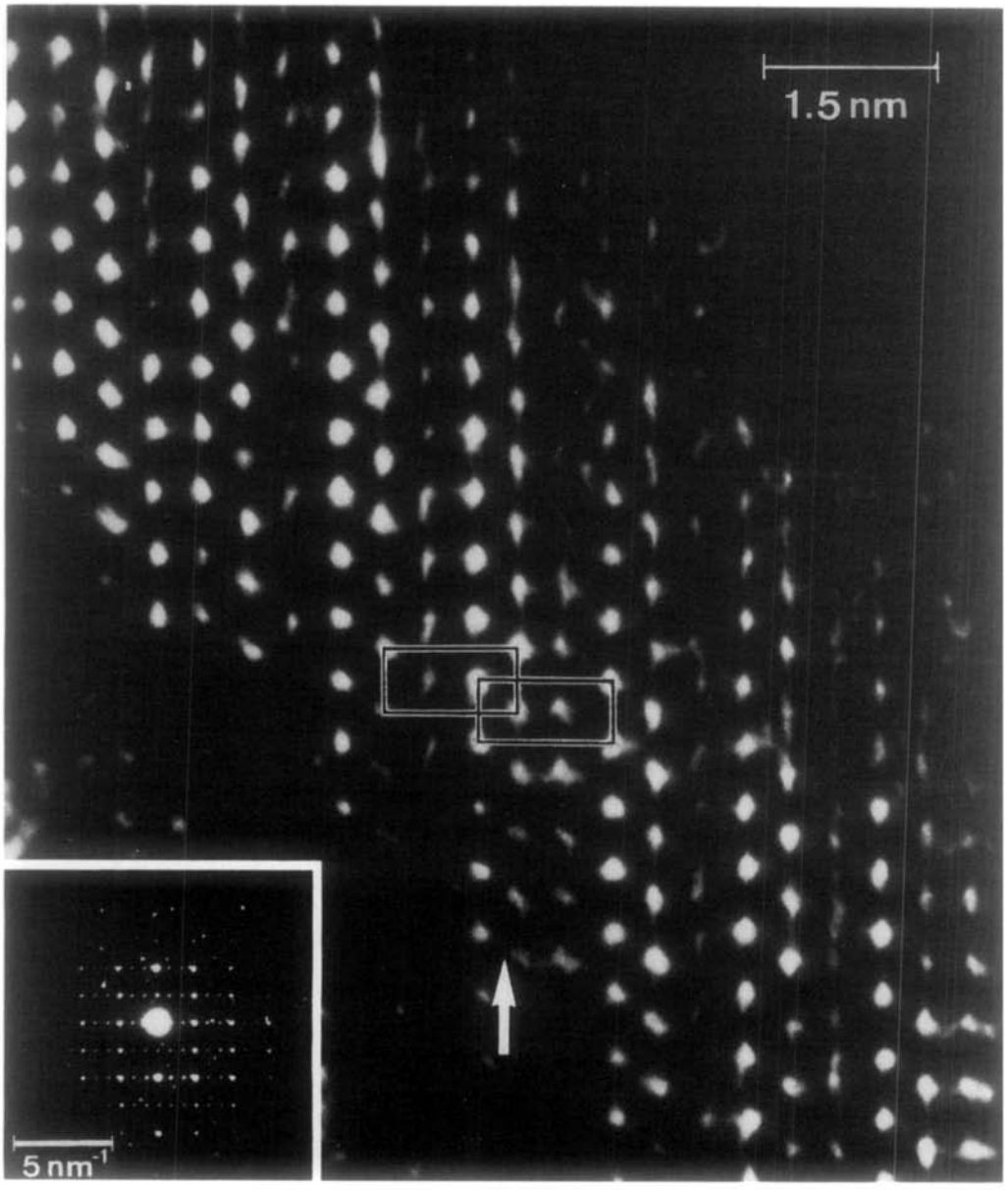

FIG. 9. HREM image with a planar defect (arrow). The imaging conditions and the rectangle in the figure are the same as those in Fig. 8.

adjacent amorphous contamination gave an underfocus value of 60 to 70 nm. Its diffraction pattern is inserted (Fig. 8b). The structure model of the $Nb_{10}Ge_7$ ordered phase projected onto the (12·0)-plane is shown in Fig. 8c. The thick circles with dots (two Nb and one Ge^{II}) correspond to the larger circle with dot (two Nb) for $Nb_5Ge_3(D8_8)$. In this figure information on the position parameter along this projection (unit thickness:

1.337 nm) is omitted. Figures 8d and 8e are calculated images using the multislice method for the ordered $Nb_{10}Ge_7$-phase and the $Nb_5Ge_3(D8_8)$-phase, respectively. The image of the ordered $Nb_{10}Ge_7$-phase (Fig. 8d) fits well to the observation (Fig. 8a), while that of Nb_5Ge_3 does not show good correspondence to the observation. Under this imaging condition, the image pattern shows the periodicity of the Ge^{II}-sublattice, although each spot does not correspond to the Ge^{II}-atom position.

7. Planar Type Defects

In Fig. 9, a planar type defect can be recognized. Since it was taken from the same negative film as Fig. 8a, the imaging conditions for both figures must be similar. Spots at corners of rectangles in the left part are the inner spots of those in the right part. The translation vector of the right part relative to the left is $[\frac{1}{3}\ \frac{2}{3} \cdot \frac{1}{2}]$, if there is no translation along the direction of observation. The spots on some of the (01·0)-planes are merging into each other. These defects on the (01·0)-plane may cause streaks such as those in Fig. 1a.

In Fig. 10, a model for the defects on the (01·0) plane with different translation vectors is constructed ([00·1]-projection), where the defects destroy the Ge^{II}-sublattices only. Models which destroy the periodicity of both the $D8_8$- and the Ge^{II}-sublattices can also be constructed. However, in these cases short interatomic distances (e.g., 0.178 nm for Nb–Nb and 0.154 nm for

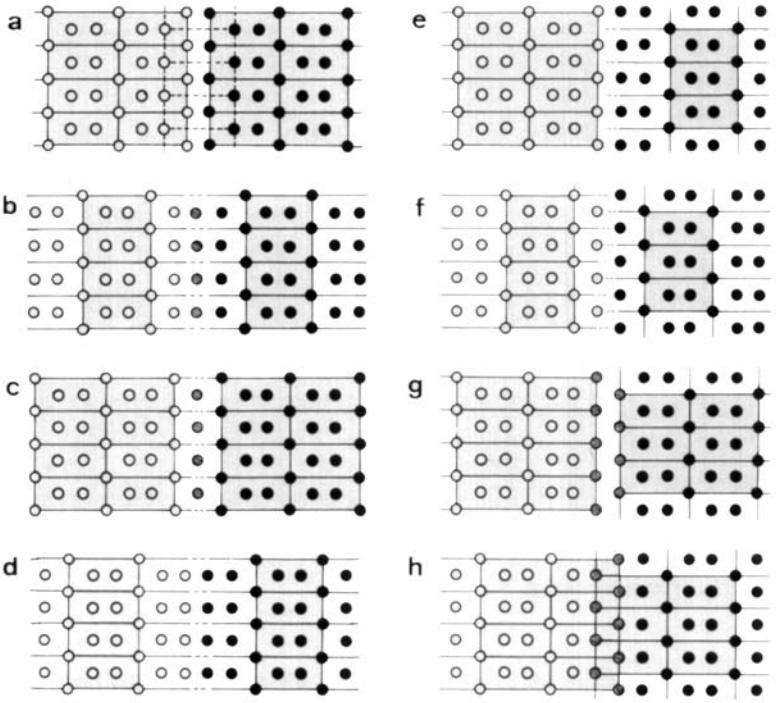

FIG. 10. Structure models of (01·0)-defects, by which only the Ge^{II}-sublattice is disturbed ([10·0]-projection), therefore only the Ge^{II}-sublattices are drawn. Black and white circles denote Ge^{II}-atoms in the right and the left parts, respectively. Shaded circles denote atoms which both parts have in common. Pattern (h) corresponds to Fig. 9.

Ge–Ge) are introduced at the defect. The translation vectors of the right part relative to the left are as follows:

(a) $[\frac{2}{3}\ \frac{1}{3} \cdot 0]$ (b) $[\frac{2}{3}\ \frac{1}{3} \cdot 0]$ (c) $[\frac{1}{3}\ \frac{2}{3} \cdot 0]$

(d) $[\frac{1}{3}\ \frac{2}{3} \cdot 0]$ (e) $[0\ 0 \cdot \frac{1}{2}]$ (f) $[0\ 0 \cdot \frac{1}{2}]$

(g) $[\frac{2}{3}\ \frac{1}{3} \cdot \frac{1}{2}]$ (h) $[\frac{1}{3}\ \frac{2}{3} \cdot \frac{1}{2}]$.

In order to simplify the figures, only the Ge^{II}-sublattices are shown. In 10a to 10d, two types of defect models (i.e., those with defects destroying the whole structure and those destroying only the Ge^{II}-sublattice) are identical. The pattern of Fig. 10h could indeed be observed in Fig. 9. Figure 10a can be explained by two (h)-type defects. HREM images of the defects can be predicted from these model patterns. The local atomic configurations around Ge^{II}-atoms are the same in all the models. The direct interactions between adjacent Ge^{II}-atoms may be small since they are separated from each other by at least 0.77 nm. Therefore, these eight types of defects appear to occur with equal frequency, though only one of them was actually observed.

8. Summary and Conclusion

A new phase related to the $Nb_5Ge_3(D8_8)$-structure was observed in a Nb–Ge co-evaporated tape (40.1 at.% Ge). From the electron diffractograms and HREM images, it was concluded that its composition is $Nb_{10}Ge_7$ (or $Nb_5Ge_3^{I}Ge_{0.5}^{II}$) and its symmetry trigonal (hexagonal cell with $a = [1\bar{1}\cdot 0]_{D8_8}$, $b = [12\cdot 0]_{D8_8}$, and $c = [00\cdot 1]_{D8_8}$). A structure model of this phase was constructed by inserting these Ge^{II}-atoms *regularly* at the octahedral sites of the $D8_8$-structure. The Ge^{II}-atoms form a triangle net of edge 1.337 nm at $z = 0$, and a honeycomb net with edge length 0.771 nm at $z = \frac{1}{2}$. The structure was thus found by electron microscopy and electron diffraction data only.

Planar defects were observed on a (01·0)-plane. They may disturb the Ge^{II}-sublattice only, but not the $Nb_5Ge_3(D8_8)$ sublattice. Since the local atomic arrangement around the defect is the same as that of any perfect crystal region, the defect energy may be low.

The grains of this phase were found to be usually elongated along the *c*-axis. This axis may be the preferential growth direction of this phase.

In this work, an ordered phase was constructed by regularly inserting Ge-atoms at octahedral sites of the $D8_8$-phase. By similar modeling (i.e., regularly inserting atoms at octahedral sites of $D8_8$-phase), various related structures (with different germanium concentrations and/or unit cell sizes) can be constructed and the existence of such materials can be predicted. This idea may be applicable also for inserting light impurity elements, though such structures have not yet been observed. Whenever the local configurations around the octahedral sites are the same, the formation energy of the ordered structures must be similar.

Acknowledgments

We are grateful to Dr. T. Ishimasa, Mr. M. Stenzel, Dr. K. Kifune, and Dr. M. Takata for helpful discussions, and to Mr. R. Wessicken and Mr. P. Wägli for technical assistance. The image calculations were performed using a DEC10 computer at the Zentrum für interaktives Rechnen, ETH-Zürich. Financial support for M.A. from Schweizerische Volkswirtschaftsstiftung is gratefully acknowledged.

References

1. J. H. Carpenter and A. W. Searcy, *J. Amer. Chem. Soc.* **78,** 2079 (1956).
2. H. Nowotny, A. W. Searcy, and J. E. Orr, *J. Phys. Chem.* **60,** 677 (1956).
3. K. Kloska and E. L. Haase, *J. Less-Common Met.* **99,** 241 (1984).
4. J. Steinmetz and B. Rosques, *C.R. Acad. Sci., Sér. C* **283,** 633 (1976).
5. W. Reiger, H. Nowotny, and F. Benesovsky, *Monatsh. Chem.* **96,** 98 (1965).
6. R. Horyń and R. Kubiak, *Bull. Acad. Pol. Sci., Sér. Sci. Chim.* **19,** 185 (1971).

7. M. PÖTZSCHKE AND K. SCHUBERT, *Z. Metallkd.* **53,** 474 (1962).
8. J. L. JORDA, R. FLÜKIGER, AND J. MÜLLER, *J. Less-Common Met.* **62,** 25 (1978).
9. H. NOWOTNY, E. PARTHÉ, R. KIEFFER, AND F. BENESOVSKY, *Monatsh. Chem.* **85,** 255 (1954).
10. R. KIEFFER, F. BENESOVSKY, AND B. LUX, *Planseeber.* **4,** 30 (1956).
11. E. PARTHÉ, W. JEITSCHKO, AND V. SADAGOPAN, *Acta Crystallogr.* **19,** 1031 (1965).
12. P. W. BROWN AND F. J. WORZALA, *J. Less-Common Met.* **41,** 77 (1975).
13. R. FLÜKIGER AND J. L. JORDA, *Solid State Commun.* **22,** 109 (1977).
14. R. FLÜKIGER, J. L. STAUDENMANN AND P. FISCHER, *J. Less-Common Met.* **50,** 253 (1976).
15. M. KONRAD, KfK Report 3244, Kernforschungszentrum Karlsruhe, Karlsruhe, FRG (1981).
16. Y. KITANO, H.-U. NISSEN, W. SCHAUER, AND D. YIN, "Proc. 17th Int. Conf. Low Temp. Phys.," Part 1, p. 615, Karlsruhe (1984).
17. Y. KITANO, H.-U. NISSEN, R. WESSICKEN, D. YIN, AND W. SCHAUER, *J. Appl. Phys.* **58,** 1904 (1985).
18. M. STENZEL, Diploma thesis, Univ. Karlsruhe and Kernforschungszentrum Karlsruhe, Inst. für Tech. Phys., Karlsruhe, FRG (1985).
19. D. YIN AND W. SCHAUER, KfK-Internal Report, 03.05.02 P01E, Kernforschungszentrum Karlsruhe, Karlsruhe, FRG (1982).
20. D. YIN, W. SCHAUER, AND F. WÜCHNER, *IEEE Trans. Magn.* **MAG 19,** 276 (1983).
21. T. ISHIMASA AND Y. FUKANO, *Japan. J. Appl. Phys.* **22,** 6 (1983).